Applied Clay Science 96 (2014) 67–72

Contents lists available at ScienceDirect

Applied Clay Science

journal homepage: www.elsevier.com/locate/clay

Research paper

Organoclay polypropylene nanocomposites under different electric field strengths

Zbigniew Rozynek [a,*,1], Suédina Maria de Lima Silva [b], Jon Otto Fossum [a,*], Geraldo José da Silva [c], Eduardo Novais de Azevedo [d], Henrik Mauroy [e], Tomás S. Plivelic [f]

[a] Department of Physics, NTNU, Høgskoleringen 5, NO-7491 Trondheim, Norway
[b] Departamento de Engenharia de Materiais, Universidade Federal de Campina Grande, 58429900 Campina Grande, PB, Brazil
[c] Instituto de Física, Universidade de Brasília, 70.919-970, Brasília, DF, Brazil
[d] Núcleo de Tecnologia, Centro Acadêmico do Agreste, Universidade Federal de Pernambuco, 55002-970 Caruaru, PE, Brazil
[e] Physics Department, IFE, P.O. Box 40, N-2027 Kjeller, Norway
[f] MAX IV Laboratory, Lund University, Box 118, SE-22100 Lund, Sweden

ARTICLE INFO

Article history:
Received 31 October 2013
Received in revised form 1 February 2014
Accepted 18 March 2014
Available online 18 April 2014

Keywords:
Clay mineral
Alignment
Polymer
Nanocomposite
Electric field
Exfoliation

ABSTRACT

Functionalities of clay-polymer nanocomposites (CPN) are related to the degree of clay particle exfoliation and orientation within the polymer matrix. Exploration of new physical methods for such CPN processing is currently an active field of research. In the present work, organoclay polypropylene nanocomposites were prepared by melt intercalation and subsequently exposed to an electric field (E) and studied in-situ by means of synchrotron X-ray scattering. Experiments were performed both at room temperature, and in the melted state (up to 200°C) and during solidification (cooling down to room temperature). Structural changes and time evolution of the alignment of the layered silicates at different E-field strengths, as well as, the final degree of their orientation is discussed. Despite many efforts, i.e. applying different E-field strengths, frequencies, and temperatures; E-field-induced clay particle exfoliation was not observed. The final state of the solidified sample is a semi-crystalline polymer matrix with embedded aligned clay particles having intercalated morphologies. E-field-assisted control of clay layers exfoliation in polymer matrices remains challenging.

1. Introduction

In this work clay mineral particles are added as nano-fillers to polymer matrices. The increase in separation of the layered structure of the clay mineral in part or in whole, known respectively as intercalation and exfoliation, produces layers, which have large specific surface area, and this in turn allows for efficient load transfer from the matrix, and enhancement in stiffness and strength. Dispersed layers also act as barriers to diffusion increasing the tortuosity of the path and inhibiting the flow of gases (Wang et al., 2006). Several chemical approaches have been utilized to prepare clay-polymer nanocomposites (CPN), including in-situ polymerization (Sun and Garces, 2002; Mauroy et al., 2013a,b) and direct melt intercalation. For the polypropylene (PP) matrix, a proper compatibility between the polymer and the clay mineral surface requires modification of the polymer with maleic anhydride (MAPP) or hydroxyl groups (HOPP) (Liu and Wu, 2001; Nam et al., 2001). It would be beneficial if the dispersion and alignment of exfoliated clay layers within polymeric matrices were achieved without chemical modification. Therefore other methods have been investigated including mechanical shearing (Okamoto et al., 2001; Murata and Haraguchi, 2007). A relatively novel idea was explored (Kim et al., 2003) using the effect of an external electric field to assist the penetration the polymer chains into the interlayer spaces that led to clay mineral exfoliation. An electric field (AC-60 Hz, 1 kVmm^{-1}) is applied on clay PP melts between the parallel layers of a rheometer, resulting in the increase of the rheological properties and exfoliation (Kim et al., 2003). However, the explanation for this behaviour was not provided within the article. Further measurements performed by the same group led to the conclusion that the exfoliation process prevails in the AC field due to the imbalance between the van der Waals attraction and the electrostatic repulsion, originating from the dissociation of the bound ions from the clay mineral surfaces (Kim et al., 2006; Park et al., 2006). In these two latter reports the clay PP nanocomposites were investigated by means of X-ray scattering in the presence of both DC and AC electric fields without any mechanical shear. Thus, a time-dependent clay exfoliation in the AC case was reported to occur purely due to the electric effects. The clay mineral alignment was also studied by the same group. They found a very strong DC electric field dependence on the clay mineral alignment, while for the AC electric fields;

* Corresponding authors.
E-mail addresses: zbigniew.rozynek@ntnu.no (Z. Rozynek), jon.fossum@ntnu.no (J.O. Fossum).
[1] Present address: Institute of Physical Chemistry, Polish Academy of Sciences, Kasprzaka 44/52, 01-224 Warsaw, Poland.

http://dx.doi.org/10.1016/j.clay.2014.03.011
0169-1317/

the particle alignment was considerably smaller and was decreasing with time, as exfoliation progressed.

These interesting phenomena were the main motivation for conducting similar experiments and understanding the mechanisms behind the *E*-field manipulation of different CPN morphologies.

E-field-assisted dispersion and alignment of clay mineral particles in different surroundings have been recently actively studied. Paineau et al. (2012) have shown how to produce novel hydrogel-based polymer-clay nanocomposites in which clay mineral layers are perfectly exfoliated and aligned by means AC *E*-fields. Alignment of clay mineral particles in various carrier fluids has been extensively studied (Rozynek et al., 2013b), including various oils (Fossum, 2012; Fossum et al., 2006; Meheust et al., 2011; Dommersnes et al., 2013; Rozynek et al., 2013c), and oligomers (Rozynek et al., 2013a).

2. Samples, experimental set-up and techniques

2.1. Sample preparation

A commercial grade of isotactic polypropylene PP H103 (Braskem, Brazil), with melt flow index 40 g/10 min at 230°C/2.16 kg and density 0.905 g/cm^3, was used as polymer matrix for CPN preparation. This grade is appropriate for injection moulding of thin walls products and, according to the manufacturer, contains heat stabilizers to protect against thermal degradation during compounding and processing. The organoclay used in this study (Cloisite® 20A) was obtained from Southern Clay Products (Gonzales, TX). It is a Na^+— montmorillonite, chemically modified with dimethyl dihydrogenated tallow quaternary ammonium chloride. Organoclay PP nanocomposites master batches were prepared in an intensive internal mixer (Haake Rheocord 90) at 50 rpm for 10 min after organoclay feeding at 210°C. Polymer and organoclay C20A were dried in a vacuum oven at 80°C for 24 h before melt mixing. The master batches were pelletized and dried for 2 h in the same conditions described above before being added to PP in order to obtain compounds with 5 mass% organoclay. These compounds were extruded in a counter-rotating twin screw extruder accessory (TW 100) coupled to a Haake operating at 60 rpm and with a temperature profile in the 150–210°C range. After extrusion, the materials were air cooled, ground and then injection moulded in a Ray Ran machine at 210°C, and 100 Pa/cm^2 of pressure for 5 seconds.

2.2. Experimental set-up and techniques

Initial synchrotron small-angle X-ray scattering (SAXS) experiments were performed at the beamline D02A of LNLS in Campinas, Brazil. These experiments were the base for the SAXS results reported here, which were all performed at the I711 beamline at MAX-lab, Sweden. The beamline was equipped with a CCD detector with 165 mm active area. The SAXS patterns were recorded using a two-dimensional detector located 67 cm from the sample. An X-ray beam with a wavelength of 1.1 Å was used, which enabled detection of scattering in a q-range of approximately 0.02–0.6 Å^{-1}. AC electric fields up to 2 kVmm^{-1} and frequency of 10, 100 and 1000 Hz, and a DC electric field of 1 kVmm^{-1} were applied using a function generator (TG215 ThurlbyThandar Instruments) and a high voltage amplifier (AS-3B1 Matsusada Precision Inc.). The two copper electrodes had a height of 7 mm and a width of 2 mm, and they were separated by a 2 mm gap. An electric field was applied in the horizontal direction and perpendicular to the X-ray beam direction. A schematic of the experimental set-up is shown in Fig. 1. A custom-made heating cell consisting of a two-wall heating unit was used to ensure the smallest temperature gradient between sample and environment. The sample chunks were placed in-between copper electrodes and thin mica elements glued to the flat sides of the electrodes using high temperature resistant glue.

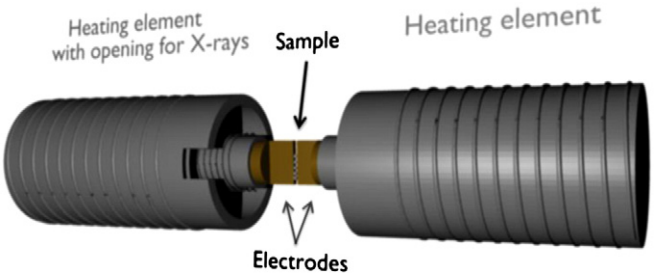

Fig. 1. Experimental set-up for SAXS measurements. Sample is placed between two copper electrodes. Two heating units are used to ensure the smallest temperature gradient between sample and environment.

3. Results and discussion

3.1. Structural changes

The structural changes of two samples exposed to DC (Sample 1) and AC (Sample 2) electric fields were monitored during melting and solidification. Samples were kept in the melted state for more than 1 h at around 200°C before application of the *E*-fields.

3.1.1. SAXS patterns and the azimuthal integration

Examples of the 2-D SAXS patterns are shown in Fig. 2. These were collected from organoclay PP sample without (left) and with (right) an AC *E*-field of 1 kVmm^{-1} applied, respectively. Prior to the application of the electric field, the organoclay particles are randomly dispersed into the melted polymeric matrix. The alignment of clay mineral particles with their stacking direction being normal to the *E*-field direction (horizontal) is observed after its application. Both the scattering at small angles and diffraction rings (P1 and P2) become anisotropic, i.e. the lowest scattering intensity is found at $\varphi \sim 0°$ and 180°, whereas it peaks at $\varphi \sim 90°$ and 270°.

All the 2-D SAXS patterns (raw data) have been processed prior to the integration, i.e. SAXS images of both the organoclay PP nanocomposite inside the sample cell and the background image of the empty sample cell were normalized by their transmissions followed by background subtraction. The contribution from pure PP was also taken into account (diffractograms of pure PP at each temperature were subtracted from the organoclay PP nanocomposite corrected data), and then the beam stop and its holder were masked out.

In Fig. 3 are shown, azimuthally averaged 2-D SAXS patterns of the organoclay PP nanocomposite during melting (left panel), and exposure to the electric fields (right panel). The position of maximum intensity, q_m, and the width of the basal reflections were found by fitting to Pseudo-Voigt profiles (solid lines). The scattering intensities were plotted against the momentum transfer $q = (4\pi/\lambda)\sin\theta$, where 2θ denotes the scattering angle and λ is the wavelength of the X-rays. The average d-value was calculated as $d = 2\pi/q_m$.

3.1.2. Samples at RT

Two major broad peaks (P1 and P2) are observed with their centres located at around $q_1 = 0.16$ and $q_2 = 0.38$ Å^{-1} for both samples in a solid form at ~25°C (the initial state: t = 1 min), and these correspond to the real space distances around $d_1 = 4.0$ and $d_2 = 1.7$ nm, respectively. The former reflection (P1) is attributed to *polymer chains intercalation* between the organoclay layers which increased the initial interlayer space $d_{Clo} = 2.4$ nm of pure Cloisite®20A organoclay (Nam and Son, 2010). The reduction of attractive forces between the clay mineral layers due to the chemical treatment of clay mineral particles (surfactant intercalation) and the presence of polar functional groups (maleic anhydride) in PP enabled the polymer chains to intercalate into the clay mineral interlayer space and changed the initial d-value $d_{Clo} = 2.4$ to $d_1 = 4.0$ nm. It should be noted that the distribution of

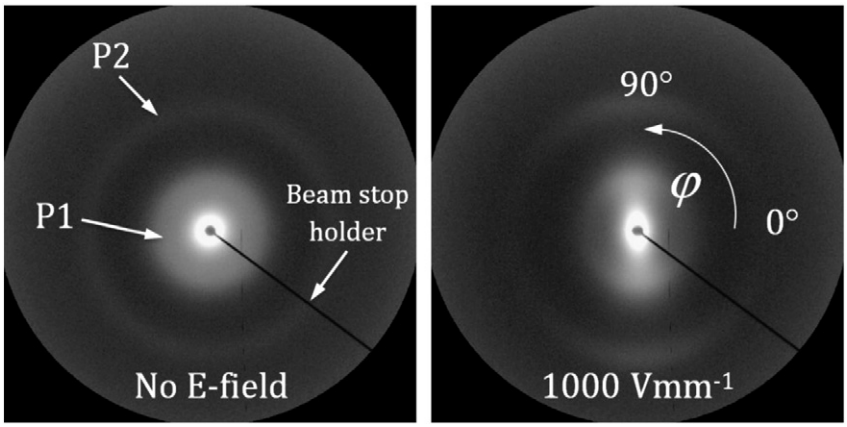

Fig. 2. 2-D SAXS images of a PP-organoclay nanocomposite in melted state (around 200°C) before (left) and after (right) application of an AC electric field of 1 $kVmm^{-1}$, 100 Hz for 5 min. Strong anisotropy can be seen in the right image. The direction of the AC *E*-field is horizontal.

the d_1 values is very broad, thus structures with some degree of disorder were obtained. The second reflection (P2) can be assigned to either the presence of a small amount of non-modified montmorillonite ($d_{Mt} = 1.2$ nm) particles acting as an impurity in a commercial product (Riva et al., 2002) or another (more likely) explanation could be that the initial Cloisite®20A structure collapsed to the bilayer and monolayer arrangement of the alkyl chains during melt processing (*surfactant molecule intercalation*). Similar observations were noted by Yoon et al. (2001). Another hypothesis was suggested by Mandalia and Bergaya (2006) and also by Zhang et al. (2005). They observed the presence of three reflections in X-ray patterns of organoclay and CPN based on polyethylene (PE) and PP respectively, attributed to the (001), (002) and (003) reflections of one intercalation state. The possibility that P2 is the second order reflection of P1 is ruled out in the present case, since the *q*-values are not positioned at multiples integer of P1, and in addition the P2 reflection is significantly narrower than the P1 reflection. In order to be more conclusive at this point, one would need to employ other experimental techniques, namely FTIR and DSC. However, this is not the main subject of the current study.

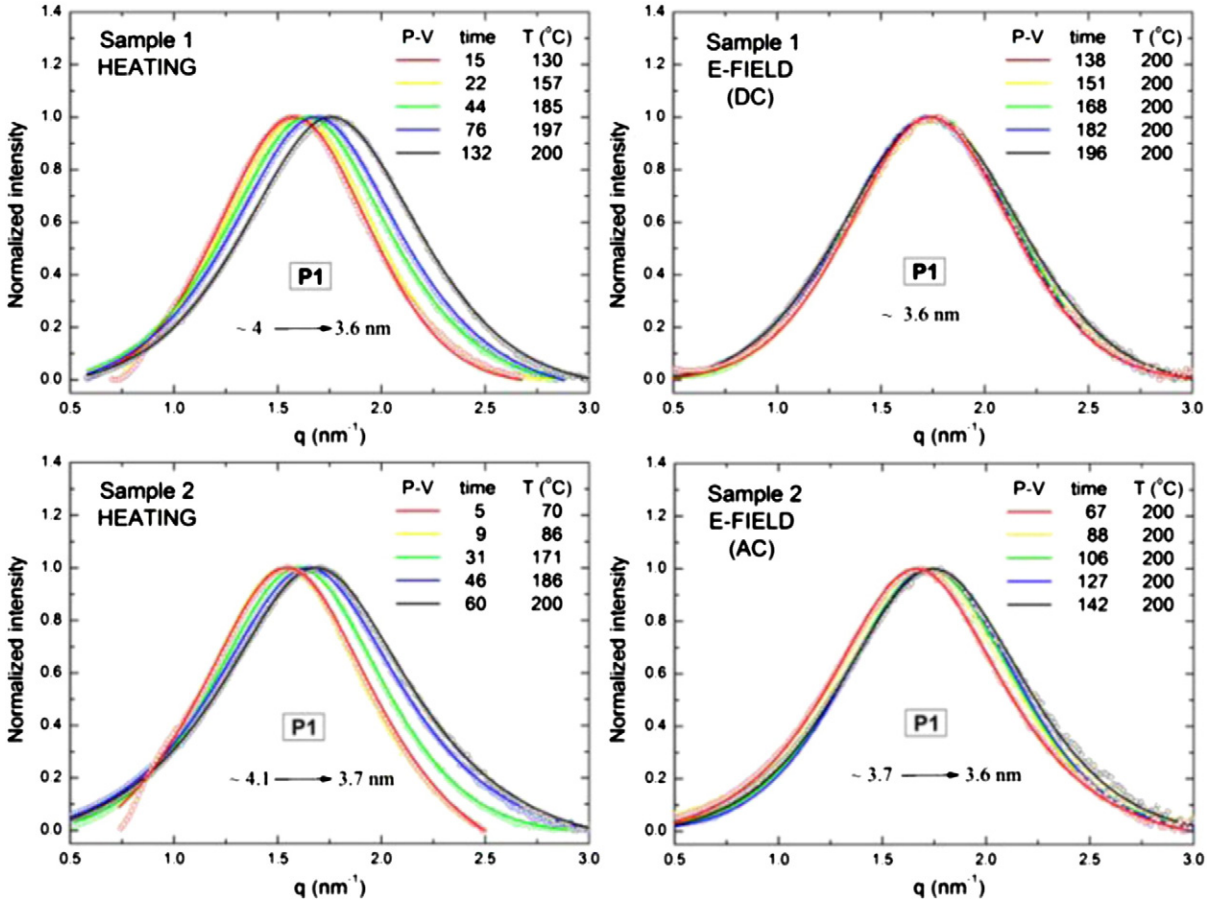

Fig. 3. Azimuthally integrated 2-D SAXS patterns of sample 1 (top) and sample 2 (bottom) during melting and temperature stabilizing (left); and *E*-field application (right). The data was fitted to Pseudo-Voigt profiles (solid lines).

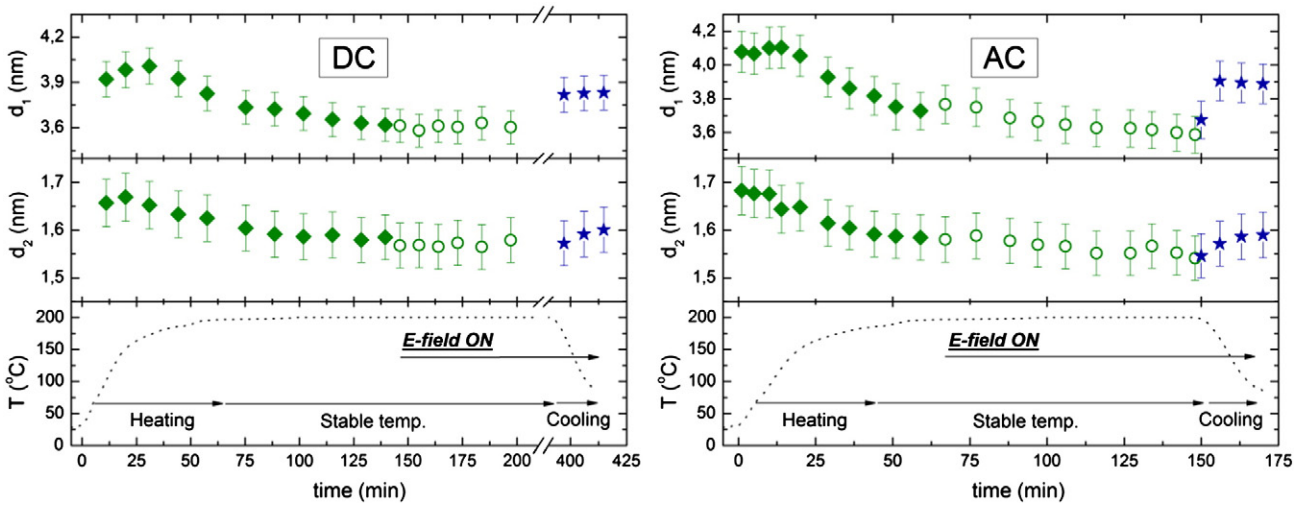

Fig. 4. Development of basal reflections related to populations of clay mineral particles with polymer d_1 and surfactant intercalated d_2 structures, respectively, as a function of time, temperature and the *E*-field presence. The dotted line shows the temperature inside the heating cell (2 mm from the sample). Filled and opened symbols represent changes in the values of the characteristic distances d_1 and d_2 for samples without and with the *E*-field applied. Cooling down of the samples is represented by blue stars.

3.1.3. Melting of the samples

Fig. 4 illustrates the development of the two characteristic distances (d_1 and d_2 associated with the reflections P_1 and P_2 respectively), as a function of time, temperature and *E*-field. During the first phase (temperature rise and stabilization) the positions of P1 and P2 clearly shift towards higher *q*-values indicating the decrease in basal reflection of two different populations of clay mineral particles, namely organoclays with polymer (d_1) and surfactant (d_2) intercalated structures, respectively. These changes are $\Delta d_1 \sim 0.4$ nm and $\Delta d_2 \sim 0.1$ nm for both samples. Since the initial values (sample at RT) of basal reflections recover (partially) rapidly during cooling (see the discussion in Section 3.1.5), it is believed that the collapse comes from the exudation of the surfactant molecules and the polymer chains out from the interlayer space during heating (Silva et al., 2007). Riva et al. (2002) and Priya and Jog (2003) have also stated that, thermodynamically, at high temperatures (>180°C), when the entropy gain due to exudation is greater than the Coulombic interaction energy between modifier and silicate layer, organic modifiers can be exuded from the interlayer space of the organoclay.

3.1.4. Samples exposed to E-fields (DC and AC) at the melted state

During the second phase (open symbols in Fig. 4) a DC *E*-field of 1 $kVmm^{-1}$ was applied to Sample 1 for about 3 h, both in the melted state and during cooling. Sample 2, however, was exposed to an AC (100 Hz) *E*-field of 1 $kVmm^{-1}$ for 60 min and then the electric field strength was increased to 2 $kVmm^{-1}$ and maintained during the cooling.

For Sample 1 (DC) both reflections remain almost at their position. The changes are within the error bars and can be considered as negligible. For Sample 2 (AC), on the other hand, both reflections P1 and P2 continue shifting in the same direction and the values of d_1 and d_2 decrease by around 0.15 nm and 0.05 nm, respectively. There is no electric field influence on the *d*-values observed, and the process seems to be time-dependent. The increase of the electric field strength (from 1 to 2 $kVmm^{-1}$) seems to have no effect on the *d*-values either (see also Supplementary Materials).

3.1.5. Cooling and solidification of the samples

In the last phase, the samples are cooled down while still exposed to *E*-fields. In case of Sample 1, the *d*-value of P1 recovers to around 3.85 nm, whereas P2 comes back to 1.6 nm. Similarly, the *d*-values from Sample 2 recover to around 3.88 nm and 1.6 nm, for P1 and P2 respectively. In both situations, the time gradient of the temperature is practically the same and the reached *d*-values become constant as the temperature is decreased below 150°C.

3.1.6. Summary

The results reported in Fig. 4 seem to indicate that the changes of *d*-values are primarily due to the temperature increase or decrease of the sample, but also this process is time-dependent. Unfortunately due to the synchrotron time restrictions it was not possible to measure for longer times (many hours or days). Also, it would be interesting to investigate the behaviour of these CPN during several heating and melting cycles.

The observations described above differ clearly from those presented by Kim et al. (2006) and Park et al. (2006). They showed that the exfoliation was due to electric field application and it was prevailed over by AC electric field rather than DC fields. In the present study, the exfoliation was not achieved. Several other samples of PCloisite®C20A-PP nanocomposites were studied at higher and lower temperatures as well as different frequencies (see Supplementary Materials) and strengths of electric fields, and the results also do not show exfoliation.

3.2. SAXS – Development of anisotropy

Application of an external electric field polarizes clay mineral particles. If the resulting electric forces overcome the homogenization effect of the temperature, particles rotate and align normal to the electric field lines with respect to their stacking direction. The alignment of particles can be monitored by means of X-ray or neutron diffraction (Knudsen et al., 2004; Rozynek et al., 2010). In order to quantify the degree of anisotropy of the system, i.e. how well the clay mineral layers aligned with respect to a specific direction, it is necessary to integrate radially over a narrow *q*-range of the 2-D SAXS patterns (see Fig. 5) and fit the obtained 1-D azimuthal plots (see Fig. 6) to a parametric function. In this paper, the Maier-Saupe model of the functional form $f(\alpha) \sim \exp(m\cos^2\alpha)$ is used. The parameter *m* quantifies the width of the distribution and α is the angle between the chosen reference direction, which is along the *E*-field, and the clay mineral particle stacking direction. The fitting parameter *m* can be expressed using the standard orientational ('nematic') order parameter (S_2). In short, the fitting parameter is related to the full width at half maxima and can be expressed as the S_2 parameter, ranging from −½ to 1, where 1 indicates perfectly oriented particles in the 'nematic' configuration, 0 states no orientation, and −½ indicates perfectly oriented particles in the 'anti-nematic' configuration

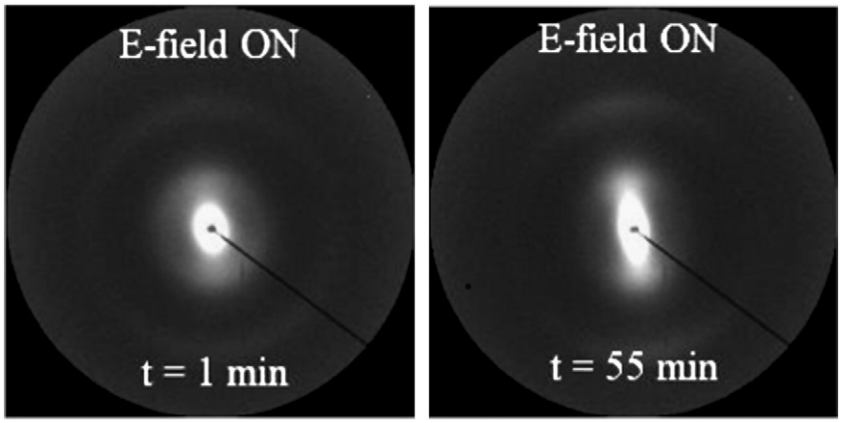

Fig. 5. 2-D SAXS images of a clay PP nanocomposite in melted state (around 200°C) under DC electric field of 1 kVmm^{-1}. Very strong anisotropy can be seen (right) after 55 min of *E*-field application. The direction of the DC *E*-field is horizontal.

(for further details see Meheust et al., 2006; Hemmen et al., 2009; Dozov et al., 2011). It is expected here that the S_2 parameter should range between 0 and -½, since the clay mineral particles align in the 'anti-nematic' fashion, i.e. the direction of the clay mineral stacks is perpendicular to the field, independently on the polar angle.

2-D SAXS images of a organoclay PP nanocomposite in melted state (around 200°C) under DC electric field of 1 kVmm^{-1} are shown in Fig. 5. The anisotropy starts to build up (left) in a direction perpendicular to the direction of the electric field lines (horizontally in the plot). Very strong anisotropy can be seen (right) after 55 min of *E*-field application. Azimuthal plots of the first Bragg reflection (P_1, polymer intercalation) are shown in Fig. 6.

The degree of anisotropy grows clearly, starting immediately after the application of the electric field. The first collected data were taken within the first minute (black circles) of the X-ray exposure. The value of the S_2 parameter was calculated to be around $S_2 = -0.19$. The next integrated image is plotted using orange diamonds, and it can be seen that the full width at half maximum becomes smaller when compared to that of the first integrated plot. This is reflected in the magnitude of the S_2 parameter, which is around $S_2 = -0.28$. The further development of the degree of anisotropy is no longer evident by inspection of the azimuthal plots in Fig. 6, in particular comparison of data plotted using blue stars and green crosses. Similar azimuthal plots were obtained for Sample 2 exposed to the AC electric fields (not included here).

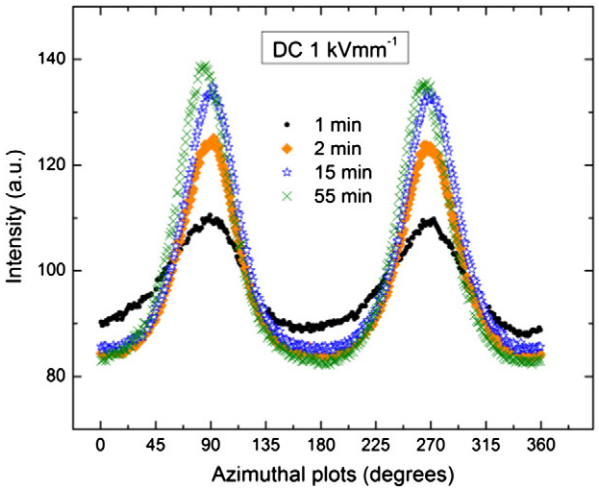

Fig. 6. Azimuthal plots of the first Bragg peak amplitude (q_1, polymer intercalation) for PP-clay sample under DC electric field of 1 kVmm^{-1}. The degree of anisotropy grows starting immediately after the application of the electric field.

The calculated values of the S_2 parameter are shown in Fig. 7. The values of S_2 in zero *E*-field are the reference values which are set to zero. It can be seen that (for both samples) the degree of anisotropy develops with time and also it depends on the temperature, and more precisely, the phase of the polymer matrix (melted vs. solidified). The time for the rotation of clay particles is directly proportional to the viscosity of the hosting medium and depends on the electric field strength that scales as $1/E^2$ (Castberg et al., 2012).

For Sample 1 (DC), the highest value of the S_2 is around −0.31 and it was achieved approximately 15 min after the application of the DC *E*-field (1 kVmm^{-1}), whereas the S_2 is around −0.3 for the last data point collected before cooling started. The polymer solidification prevents better particle orientation, and the magnitude of the S_2 parameter decreased. The final value of the S_2 was found to be around −0.26, when Sample 1 was cooled down to about 70°C.

For Sample 2 (AC), the highest value of the S_2 is around −0.3 and it was achieved approximately 25 min after the application of the AC *E*-field (1 kVmm^{-1}). The degree of anisotropy increases slightly ($\Delta S_2 \sim 0.005$) when the strength of the electric field is increased to 2 kVmm^{-1} (filled circles). Again the polymer solidification prevents better particle orientation, and the magnitude of the S_2 decreases. The final value of the S_2 was found to be around −0.285, when Sample 2 was cooled down to about 70°C.

4. Conclusions

The primary objective of this research was to investigate the structural changes and time evolution of the alignment of the layered clay minerals under different *E*-field strengths. Development of the average stacking distances as a function of time, temperature and the presence of *E*-field was measured by means of SAXS. *E*-field application has a noticeable effect on particle arrangement, which can be important for production of CPN (for example gas barrier applications). Unfortunately, no particle exfoliation to single layers was observed as previously reported (Kim et al., 2006; Park et al., 2006). While monitoring changes of the degree of anisotropy, the polymer solidification may disorganize the particle alignment, as the magnitude of the S_2 parameter decreased slightly when compared to those of the sample at a melted state. The semi-crystalline CPN after the heating and cooling cycle, present highly oriented intercalated CPN structures. Application of either DC or AC electric fields resulted in very similar particle alignment and neither of them should be considered superior.

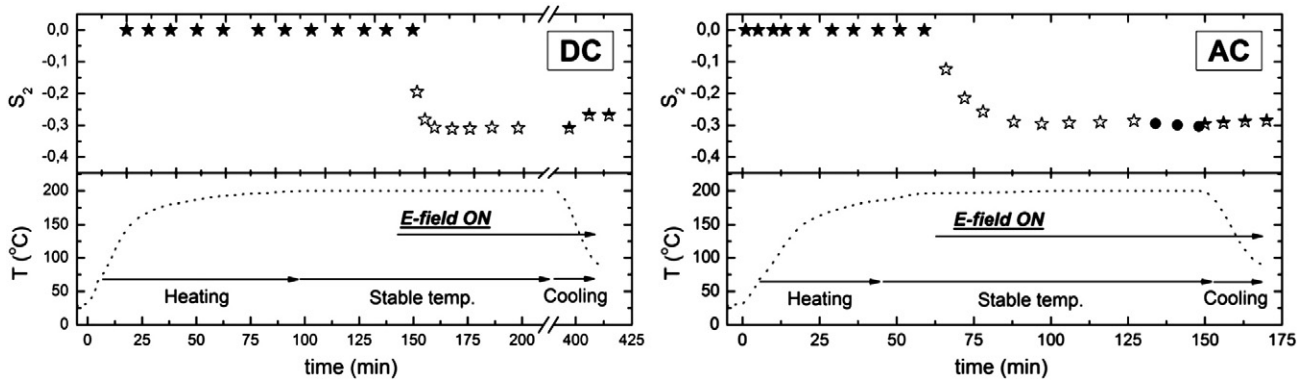

Fig. 7. Development of the degree of anisotropy as a function of time and the phase of the polymer matrix (melted vs. crystallized). A DC electric field was applied to Sample 1 (left) and an AC electric field was applied to Sample 2 (right).

Acknowledgments

The authors acknowledge assistance from D. Haase and C. B. Hansen while performing experiments at the beamline I711 at MAX-lab, Sweden, and also the staff at the SAXS beamline of LNLS. P. Hammersley the creator of the Fit2D program, is also acknowledged. We wish to thank K. Walbert for her comments that helped to improve the manuscript. This work was supported by the Research Council of Norway, MAX-lab and LNLS.

Appendix A. Supplementary data

Supplementary data to this article can be found online at http://dx.doi.org/10.1016/j.clay.2014.03.011.

References

Castberg, R., Rozynek, Z., Fossum, J.O., Maloy, K.J., Dommersnes, P., Flekkoy, E.G., 2012. Clay alignment in electric fields. Rev. Cub. Fis. 29, 17–19.
Dommersnes, P., Rozynek, Z., Mikkelsen, A., Castberg, R., Kjerstad, K., Hersvik, K., Fossum, J.O., 2013. Active structuring of colloidal armour on liquid drops. Nat. Commun. 4, 2066.
Dozov, I., Paineau, E., Davidson, P., Antonova, K., Baravian, C., Bihannic, I., Michot, L.J., 2011. Electric-field-induced perfect anti-nematic order in isotropic aqueous suspensions of a natural beidellite clay. J. Phys. Chem. B 115, 7751–7765.
Fossum, J.O., 2012. Flow of clays. Eur. Phys. J. Spec. Top. 204, 41–56.
Fossum, J.O., Meheust, Y., Parmar, K.P.S., Knudsen, K.D., Maloy, K.J., Fonseca, D.M., 2006. Intercalation-enhanced electric polarization and chain formation of nano-layered particles. Europhys. Lett. 74, 438–444.
Hemmen, H., Ringdal, N.I., De Azevedo, E.N., Engelsberg, M., Hansen, E.L., Meheust, Y., Fossum, J.O., Knudsen, K.D., 2009. The isotropic-nematic interface in suspensions of na-fluorohectorite synthetic clay. Langmuir 25, 12507–12515.
Kim, D.H., Park, J.U., Ahn, K.H., Lee, S.J., 2003. Electrically activated poly(propylene)/clay nanocomposites. Macromol. Rapid Commun. 24, 388–391.
Kim, D.H., Cho, K.S., Mitsumata, T., Ahn, K.H., Lee, S.J., 2006. Microstructural evolution of electrically activated polypropylene/layered silicate nanocomposites investigated by in situ synchrotron wide-angle x-ray scattering and dielectric relaxation analysis. Polymer 47, 5938–5945.
Knudsen, K.D., Fossum, J.O., Helgesen, G., Haakestad, M.W., 2004. Small-angle neutron scattering from a nano-layered synthetic silicate. Phys. B Condens. Matter 352, 247–258.
Liu, X.H., Wu, Q.J., 2001. Pp/clay nanocomposites prepared by grafting-melt intercalation. Polymer 42, 10013–10019.
Mandalia, T., Bergaya, F., 2006. Organo clay mineral-melted polyolefin nanocomposites - effect of surfactant/cec ratio. J. Phys. Chem. Solids 67, 836–845.
Mauroy, H., Plivelic, T.S., Hansen, E.L., Fossum, J.O., Helgesen, G., Knudsen, K.D., 2013a. Effect of clay surface charge on the emerging properties of polystyrene–organoclay nanocomposites. J. Phys. Chem. C 117, 19656–19663.
Mauroy, H., Rozynek, Z., Plivelic, T.S., Fossum, J.O., Helgesen, G., Knudsen, K.D., 2013b. Oxygen-controlled phase segregation in poly(n-isopropylacrylamide)/laponite nanocomposite hydrogels. Langmuir 29, 371–379.
Meheust, Y., Knudsen, K.D., Fossum, J.O., 2006. Inferring orientation distributions in anisotropic powders of nano-layered crystallites from a single two-dimensional waxs image. J. Appl. Crystallogr. 39, 661–670.
Meheust, Y., Parmar, K.P.S., Schjelderupsen, B., Fossum, J.O., 2011. The electrorheology of suspensions of na-fluorohectorite clay in silicone oil. J. Rheol. 55, 809–833.
Murata, K., Haraguchi, K., 2007. Optical anisotropy in polymer-clay change on uniaxial deformationt nanocomposite hydrogel and its. J. Mater. Chem. 17, 3385–3388.
Nam, B.U., Son, Y., 2010. Evaluations of pp-g-gma and pp-g-hema as a compatibilizer for polypropylene/clay nanocomposites. Polym. Bull. 65, 837–847.
Nam, P.H., Maiti, P., Okamoto, M., Kotaka, T., Hasegawa, N., Usuki, A., 2001. A hierarchical structure and properties of intercalated polypropylene/clay nanocomposites. Polymer 42, 9633–9640.
Okamoto, M., Nam, P.H., Maiti, P., Kotaka, T., Hasegawa, N., Usuki, A., 2001. A house of cards structure in polypropylene/clay nanocomposites under elongational flow. Nano Lett. 1, 295–298.
Paineau, E., Dozov, I., Bihannic, I., Baravian, C., Krapf, M.-E.M., Philippe, A.-M., Rouziere, S., Michot, L.J., Davidson, P., 2012. Tailoring highly oriented and micropatterned clay/polymer nanocomposites by applying an a.C. Electric field. ACS Appl. Mater. Interfaces 4, 4296–4301.
Park, J.U., Choi, Y.S., Cho, K.S., Kim, D.H., Ahn, K.H., Lee, S.J., 2006. Time-electric field superposition in electrically activated polypropylene/layered silicate nanocomposites. Polymer 47, 5145–5153.
Priya, L., Jog, J.P., 2003. Intercalated poly(vinylidene fluoride)/clay nanocomposites: Structure and properties. J. Polym. Sci. B Polym. Phys. 41, 31–38.
Riva, A., Zanetti, M., Braglia, M., Camino, G., Falqui, L., 2002. Thermal degradation and rheological behaviour of eva/montmorillonite nanocomposites. Polym. Degrad. Stab. 77, 299–304.
Rozynek, Z., Knudsen, K.D., Fossum, J.O., Meheust, Y., Wang, B., Zhou, M., 2010. Electric field induced structuring in clay-oil suspensions: New insights from waxs, sem, leak current, dielectric permittivity, and rheometry. J. Phys. Condens. Matter 22, 8.
Rozynek, Z., Castberg, R.C., Mikkelsen, A., Fossum, J.O., 2013a. Electric field nematic alignment of fluorohectorite clay particles in oligomeric matrices. J. Mater. Res. 28, 1349–1355.
Rozynek, Z., Mauroy, H., Castberg, R., Knudsen, K.D., Fossum, J.O., 2013b. Dipolar ordering of clay particles in various carrier fluids. Rev. Cub. Fis. 29, 37–41.
Rozynek, Z., Zacher, T., Janek, M., Caplovicova, M., Fossum, J.O., 2013c. Electric-field-induced structuring and rheological properties of kaolinite and halloysite. Appl. Clay Sci. 77–78, 1–9.
Silva, S.M.L., Lopez-Manchado, M.A., Arroyo, M., 2007. Thermoplastic olefin/clay nanocomposites. Effect of matrix composition, and organoclay and compatibilizer structure on morphology/properties relationships. J. Nanosci. Nanotechnol. 7, 4456–4464.
Sun, T., Garces, J.M., 2002. High-performance polypropylene-clay nanocomposites by in-situ polymerization with metallocene/clay catalysts. Adv. Mater. 14, 128–130.
Wang, J.F., Severtson, S.J., Stein, A., 2006. Significant and concurrent enhancement of stiffness, strength, and toughness for paraffin wax through organoclay addition. Adv. Mater. 18, 1585–1588.
Yoon, J.T., Jo, W.H., Lee, M.S., Ko, M.B., 2001. Effects of comonomers and shear on the melt intercalation of styrenics/clay nanocomposites. Polymer 42, 329–336.
Zhang, J.G., Jiang, D.D., Wilkie, C.A., 2005. Polyethylene and polypropylene nanocomposites based upon an oligomerically modified clay. Thermochim. Acta 430, 107–113.